Smart Structures and Systems, *Vol. 18, No. 1 (2016) 117-138*
DOI: http://dx.doi.org/10.12989/sss.2016.18.1.117

Innovative modeling of tuned liquid column damper controlled structures

Alberto Di Matteo[*1], Mario Di Paola[1a] and Antonina Pirrotta[1,2b]

[1]Dipartimento di Ingegneria Civile, Ambientale, Aerospaziale, dei Materiali (DICAM), Università degli Studi di Palermo, Viale delle Scienze, 90128 Palermo, Italy
[2]Department of Mathematical Sciences, University of Liverpool, Liverpool, Uk

(Received September 26, 2015, Revised April 21, 2016, Accepted May 6, 2016)

Abstract. In this paper a different formulation for the response of structural systems controlled by Tuned Liquid Column Damper (TLCD) devices is developed, based on the mathematical tool of fractional calculus. Although the increasing use of these devices for structural vibration control, it has been demonstrated that existing model may lead to inaccurate prediction of liquid motion, thus reflecting in a possible imprecise description of the structural response. For this reason the recently proposed fractional formulation introduced to model liquid displacements in TLCD devices, is here extended to deal with TLCD controlled structures under base excitations. As demonstrated through an extensive experimental analysis, the proposed model can accurately capture structural responses both in time and in frequency domain. Further, the proposed fractional formulation is linear, hence making identification of the involved parameters extremely easier.

Keywords: tuned liquid column damper; passive control; fractional derivatives; experimental investigation

1. Introduction

Tuned Liquid Column Dampers (TLCDs) are passive vibration control devices, which dissipate structural vibrations through the motion of liquid inside U-shaped containers. Classical mathematical formulation ruling the TLCD liquid displacement (Sakai *et al.* 1989) is represented by a nonlinear differential equation, whose nonlinear term describes the head losses and damping effects of the liquid motion within the container.

Due to some of their characteristics, in this decade an increasing interest in using these devices for structural vibration control purposes has been noticed (Ziegler 2007, Cheng *et al.* 2015, Lee and Juang 2012). Real applications of these systems can be observed in many countries and therefore most researches deal with the optimization of design parameters to enhance control performance (Yalla and Kareem 2000, Wu *et al*. 2012, Hochrainer and Ziegler 2006, Ziegler 2008, Di Matteo *et al*. 2014a, 2015a).

However, just dealing with the motion of the liquid inside the TLCD, it has been recently

∗Corresponding author, Ph.D., E-mail: alberto.dimatteo@unipa.it
[a] Professor, E-mail: mario.dipaola@unipa.it
[b] Professor, E-mail: antonina.pirrotta@unipa.it

http://www.techno-press.org/?journal=sss&subpage=8 ISSN: 1738-1584 (Print), 1738-1991 (Online)

proved (Chaiviriyawong *et al.* 2007, Wu *et al.* 2009, Lee *et al.* 2012, Hitchcock *et al.* 1997) that existing classical nonlinear mathematical model can be inaccurate in predicting surface liquid displacement, unless particular devices geometry are considered. In fact, for some geometric TLCD configurations, experimental tests have shown remarkable discrepancies between predicted and experimentally recorded natural frequencies of liquid oscillation.

Specifically, in a recent work (Di Matteo *et al.* 2015b) it has been pointed out that when sloshing motion occurs (Ibrahim 2005), together with vertical motion, the apparent natural frequency of liquid oscillation departs from the theoretical one.

Classical formulation does not take into account this feature, which instead has been well predicted through an innovative formulation obtained introducing a fractional derivative term. In fact, as well assessed in (Spanos and Evangelatos 2010), a fractional dissipative term acts on both damping and stiffness, leading to a simultaneous alteration of both the resonant frequency and the degree of damping of the system.

It has then been proved (Di Matteo *et al*. 2015b) that a linear fractional differential equation can highly capture the real behavior of the free surface liquid motion of TLCD devices, without a valve or an orifice inside. However this recent study, and related experimental results, was only focused on the TLCD device, and not on the whole structural system equipped with TLCD.

In this regard aim of this paper is the extension of the aforementioned formulation to predict structural system response. Note that this proposed formulation, due to its linearity, could represents a valid improvement of the classical nonlinear equation of motion, since it leads to a much simpler parameters identification than the classical nonlinear formulation. Unknown parameters can, in fact, be easily determined in the frequency domain as in any linear system.

Further, in order to fully validate the proposed formulation, experimental tests have been conducted in the Laboratory of Experimental Dynamic at University of Palermo. Numerical results obtained with the proposed fractional formulation have been compared with the corresponding experimental ones and numerical results computed with the classical formulation, proving the reliability of the fractional derivative model.

2. Problem formulation

2.1 Classical theoretical model

Consider a TLCD device as shown in Fig. 1(a), driven by a base acceleration $\ddot{x}_g(t)$. During the motion, the liquid inside the vertical columns is assumed to move vertically relative to the tube with an average velocity $\dot{y}(t)$. From the continuity equation, the average horizontal liquid velocity in the horizontal duct is $\nu\dot{y}(t)$, where $(\nu = A_v/A_h)$ is the ratio between A_v, the vertical duct cross-sectional area, and A_h, the horizontal duct cross-sectional area.

Using energy principles, the Lagrange equation yields the equation of motion of the liquid displacement $y(t)$ as

$$\ddot{y}(t)+\frac{1}{2}\frac{\xi}{L_e}\nu\left|\dot{y}(t)\right|\dot{y}(t)+\omega_e^2 y(t)=-\frac{b}{L_e}\ddot{x}_g(t) \tag{1}$$

where $(L_e = 2h + \nu b)$ is defined as the effective liquid length, h and b are the vertical and horizontal liquid length respectively (see Fig. 1(a)), ξ is the so-called head loss coefficient and

$$\omega_e = \sqrt{\frac{2g}{L_e}} \tag{2}$$

is the natural frequency of liquid oscillation inside the TLCD, with g the gravitational constant. Clearly, if the simple case of uniform cross section $(A_h = A_v = A = d \cdot s)$ is considered, then $(\nu = 1)$ and $(L_e = L = 2h + b)$, which represents the total length of the liquid inside the TLCD.

Note that Eq. (1) is a nonlinear differential equation, in which the nonlinear term appears to take into account the hydrodynamic head losses and viscous interactions which arise during the motion of the liquid inside the TLCD device (Hitchcock *et al*. 1997, Wu *et al.* 2009).

Consider now a shear-type single-degree-of-freedom structure (main system) subjected to a base excitation, whose equation of motion can be written as

$$M\,\ddot{x}(t) + C\dot{x}(t) + Kx(t) = -M\ddot{x}_g(t) \tag{3}$$

where $x(t)$ is the relative displacement of the main system and M, C and K are the mass, damping and stiffness parameters of the main structure respectively.

Let the motion of the main system be controlled through a TLCD device (see Fig. 1(b)). Then the corresponding classical governing equations (Sakai *et al*. 1989) of the aforementioned system are

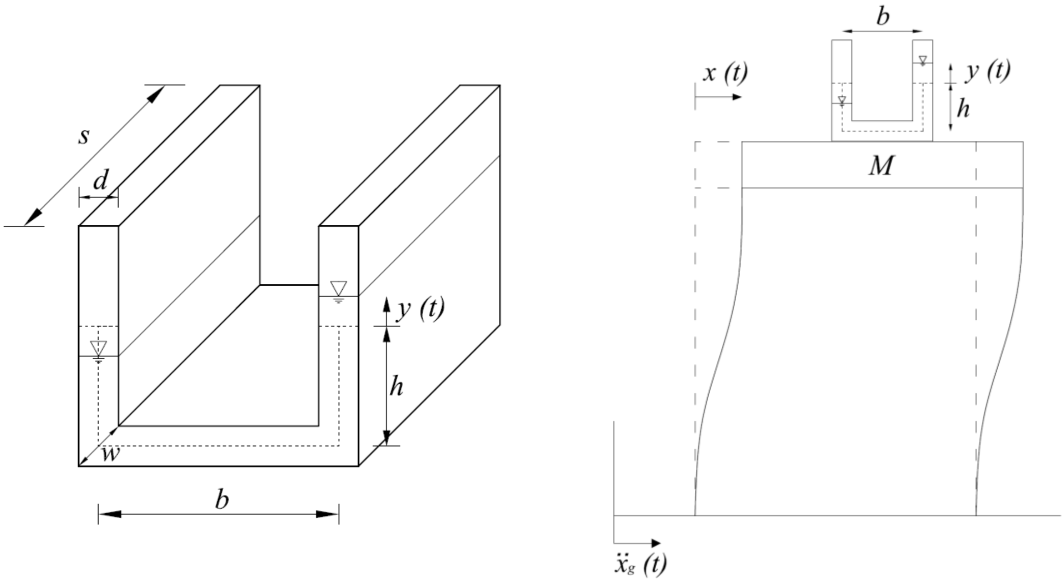

(a) TLCD device (b) TLCD controlled system

Fig. 1 Systems corresponding to Eq. (1) and (4)

$$\begin{cases} (M+m)\ddot{x}(t)+m_h\ddot{y}(t)+C\dot{x}(t)+Kx(t)=-(M+m)\ddot{x}_g(t) \\ m_h\ddot{x}(t)+m\ddot{y}(t)+\frac{1}{2}\rho A\xi|\dot{y}(t)|\dot{y}(t)+2\rho Agy(t)=-m_h\ddot{x}_g(t) \end{cases} \tag{4 a,b}$$

where $(m=\rho AL)$ represents the total liquid mass in the TLCD device, $(m_h=\rho Ab)$ is the liquid mass of the horizontal portion only and ρ is the liquid density.

Further, dividing Eq. (4(a)) by M and Eq. (4(b)) by m, Eq. (4) can be recast in canonical form as

$$\begin{cases} (1+\mu)\ddot{x}(t)+\alpha\mu\ddot{y}(t)+2\zeta_1\omega_1\dot{x}(t)+\omega_1^2x(t)=-(1+\mu)\ddot{x}_g(t) \\ \alpha\ddot{x}(t)+\ddot{y}(t)+\frac{\xi}{2L}|\dot{y}(t)|\dot{y}(t)+\omega_e^2y(t)=-\alpha\ddot{x}_g(t) \end{cases} \tag{5 a,b}$$

where $(\zeta_1=C/2M\omega_1)$ and $(\omega_1^2=K/M)$ are the damping coefficient and natural frequency of the main structure respectively, $(\mu=m/M)$ is the mass-ratio between the liquid and the main structure, and $(\alpha=b/L)$.

2.2 Proposed theoretical model

The vast majority of studies in literature have resorted to Eqs. (4) and (5) to model the motion of TLCD controlled structures under a ground excitation. Based on these relations, many research efforts have been then devoted to the determination of the optimal values of head loss coefficient ξ and theoretical liquid natural frequency ω_e for design purposes.

Recent works have pointed out that discrepancies may arise between the theoretical natural frequency ω_e in Eq. (2) and the experimentally determined one, obviously leading to differences between experimental and numerical results in time domain as well.

Specifically aforementioned discrepancies may be ascribable to several phenomena, not considered in the classical formulation, such as variation of the liquid velocity in case of large transition zones between vertical and horizontal part of the TLCD device, vortices and separation in the flow induced by liquid viscosity, sloshing effects of the liquid in the vertical columns (Wu *et al.* 2005, Konar *et al*. 2012) and sharp edge effects in case of sharp corners (Lee *et al*. 2012).

As for instance shown in Wu *et al*. (2005), in case of broadband noise ground excitation TLCD free water surface may simultaneously experience vertical displacements and a sloshing motion, leading to deviation of the measured liquid frequency from the theoretical one.

To take into account these phenomena, in (Di Matteo *et al.* 2015b) a different equation of motion, ruling the evolution of the free surface liquid displacements, has been introduced. Specifically, replacing the nonlinear damping term in Eq. (1) with a fractional derivative term, yields the equation of motion of the liquid displacement $y(t)$ as

$$\ddot{y}(t)+\frac{1}{2}\frac{C_\beta}{L}\left({}_0^C D_t^\beta y(t)\right)+\omega_e^2y(t)=-\frac{b}{L}\ddot{x}_g(t) \tag{6}$$

where C_β is a constant that can be considered as a fractional damping coefficient and $\left({}_0^C D_t^\beta y(t)\right)$ is a β-order left Caputo fractional derivative, defined as (Podlubny 1999)

$$
{}_0^C D_t^\beta y(t) = \frac{1}{\Gamma(1-\beta)} \int_0^t (t-\tau)^\beta \frac{d}{d\tau} y(\tau) d\tau, \quad 0 < \beta < 1 \tag{7}
$$

being $\Gamma(\bullet)$ the Euler-Gamma function.

Note that Eq. (6) contains only linear terms, hence it is now a linear differential equation, albeit of fractional order.

Resorting to the Fourier transform property of fractional derivatives, that is

$$
\mathscr{F}\left({}_0^C D_t^\beta y(t)\right) = (i\omega)^\beta \mathscr{F}\left(y(t)\right) \tag{8}
$$

the liquid displacement Frequency Response Function (FRF) $\left(H_y(\omega) = Y(\omega) / \ddot{X}_g(\omega)\right)$ may be easily obtained from Eq. (6) as

$$
H_y(\omega) = \frac{-\dfrac{b}{L}}{-\omega^2 + \dfrac{1}{2}\dfrac{C_\beta}{L}(i\omega)^\beta + \omega_e^2} \tag{9}
$$

Observe that Eq. (9) can be used to identify the two unknown parameters C_β and β, for instance through a best fitting procedure on the experimentally evaluated liquid displacement FRF. As soon as these two parameters are identified, Eq. (6) can be solved numerically leading to the liquid motion time history $y(t)$. This procedure has been applied in (Di Matteo *et al.* 2015b), showing that Eq. (6) yields differences between numerical and experimental liquid motion time histories considerably smaller than those obtained through the classical equation of motion Eq. (1).

However, in that paper attention was focused on the modeling of the liquid motion inside the device only.

To extend those results for TLCD controlled systems, proceeding as in (Di Matteo *et al.* 2015b), the nonlinear damping term in Eq. (5(b)) can be replaced with a Caputo fractional derivative term, leading to the sought equations of motion in the form

$$
\begin{cases}
(1+\mu)\ddot{x}(t) + \alpha\mu\ddot{y}(t) + 2\zeta_1\omega_1\dot{x}(t) + \omega_1^2 x(t) = -(1+\mu)\ddot{x}_g(t) \\
\alpha\ddot{x}(t) + \ddot{y}(t) + \dfrac{1}{2}\dfrac{C_\beta}{L}\left({}_0^C D_t^\beta y(t)\right) + \omega_e^2 y(t) = -\alpha\ddot{x}_g(t)
\end{cases} \tag{10 a,b}
$$

Note that Eq. (10) is now a system of linear coupled differential equations, the second of which is of fractional order.

Further, Fourier transforming Eq. (10) and taking into account Eq. (8) yields

$$\begin{cases} -\omega^2(1+\mu)X(\omega)-\omega^2\alpha\mu Y(\omega)+2i\omega\zeta_1\omega_1 X(\omega)+\omega_1^2 X(\omega)=-(1+\mu)\ddot{X}_g(\omega) \\ -\omega^2\alpha X(\omega)-\omega^2 Y(\omega)+(i\omega)^\beta \dfrac{C_\beta}{2L}Y(\omega)+\omega_e^2 Y(\omega)=-\alpha\ddot{X}_g(\omega) \end{cases} \tag{11 a,b}$$

Thus, the structural displacement FRF $\left(H_x(\omega)=X(\omega)/\ddot{X}_g(\omega)\right)$ can be written as

$$H_x(\omega)=\frac{1+\mu+\dfrac{\omega^2\alpha^2\mu}{B(\omega)}}{(1+\mu)\omega^2+\dfrac{\omega^4\alpha^2\mu}{B(\omega)}-2i\omega\zeta_1\omega_1-\omega_1^2} \tag{12}$$

while the liquid vertical motion FRF $\left(\tilde{H}_y(\omega)=Y(\omega)/\ddot{X}_g(\omega)\right)$ is

$$\tilde{H}_y(\omega)=\frac{\alpha}{B(\omega)}\left[\frac{2\omega\zeta_1\omega_1+\omega_1^2}{(1+\mu)\omega^2+\dfrac{\omega^4\alpha^2\mu}{B(\omega)}-2i\omega\zeta_1\omega_1-\omega_1^2}\right] \tag{13}$$

where

$$B(\omega)=-\omega^2+\frac{1}{2}\frac{C_\beta}{L}(i\omega)^\beta+\omega_e^2 \tag{14}$$

It is worth stressing that, if the main structural parameters ζ_1 and ω_1 are known, Eq. (12) can be used to identify the two unknown parameters C_β and β, through a best fitting on the experimentally evaluated structural displacement FRF. This procedure will be clearly shown in the following section.

3. Experimental investigation

In order to experimentally validate the proposed linear fractional formulation in Eq. (9), a small-scale SDOF shear-type frame, made with two steel columns and two steel plates as upper-base and floor, has been built in the Laboratory of Experimental Dynamics at University of Palermo. Further, TLCD-controlled structures have been realized with U-shaped Plexiglas® vessels rigidly connected to the upper plate of the main systems.

Two configurations of TLCDs with same horizontal liquid length b, but two different cross sectional areas A have been considered. Specifically, the diverse values of A have been obtained varying the width d and keeping constant the transversal dimension s (see Fig. 1).

Note that, in this way the ratio $(\gamma=w/b)$ between the corner to corner width $\left(w=d\sqrt{2}\right)$ and the horizontal liquid length b has been varied. As in fact demonstrated in (Chaiviriyawong et al.

2007), γ represents an important parameter since it may be one of the principal causes of discrepancies between theoretical and experimental liquid natural frequencies.

Therefore, building two different TLCD devices has allowed studying the effects of the variation of this ratio on the proposed formulation. Clearly, since two TLCD configurations have been considered, two corresponding main systems to be controlled have been built.

In the following theoretical/experimental validation of the proposed formulation on these two TLCD controlled structures is presented.

3.1 Main systems

As detailed above, since the main system has to take into account also the dead weight of the TLCD vessels, two small shear-type frames with the two empty TLCD devices on the upper plate, have been used as two main systems Configurations (#1 and #2). In Figs. 2(a) and 2(b) pictures of the two main systems configurations are shown, while in Figs. 2(c) and 2(d) schematic drawings of the structures with the corresponding dimensions are depicted.

(a) Picture of Configuration #1 (b) Picture of Configuration #2

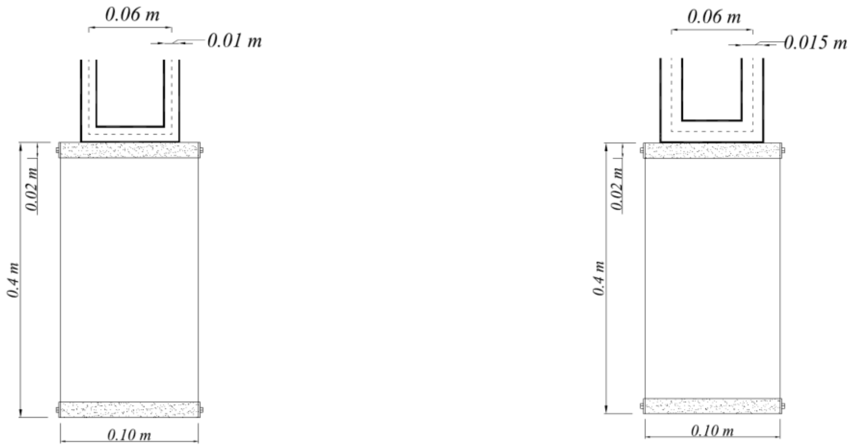

(c) Dimensions for Configuration #1 (d) Dimensions for Configuration #2

Fig. 2 Experimental setup of the main systems

As shown in these figures, here adopted TLCD devices have rather large lateral dimensions, which is suitable for laboratory testing. Clearly such a design would not be proper for real buildings, where lateral excitations cannot be excluded, leading to unwanted lateral liquid sloshing.

To experimentally identify dynamic structural parameters of the shear-type frames, the two SDOF systems have been rigidly connected and excited at the base through an APS Dynamic-Model 133 shake table (Figs. 2(a) and 2(b)). Acceleration responses, at the base and at the storey of the systems, have been acquired using Miniature DeltaTrone Accelerometers Brüel&Kjær - Type 4507-002B trough a NI PXIe-1082 DAQ device, equipped with a high-performance 16-channels NI PXIe-4497 board. Since the same device is also equipped with a NI PXIe-4497 board digital-to-analog (D/A) converter, it has been used to generate the output voltage signals for the APS shake table, thus providing the base excitation. Finally the entire system is controlled via a self-developed signal processing software in LabVIEW environment. In Fig. 3 the principal devices used for the shake table tests are presented, while Fig. 4 shows an outline of the experimental setup.

Fig. 3 Acquisition devices for shake table tests

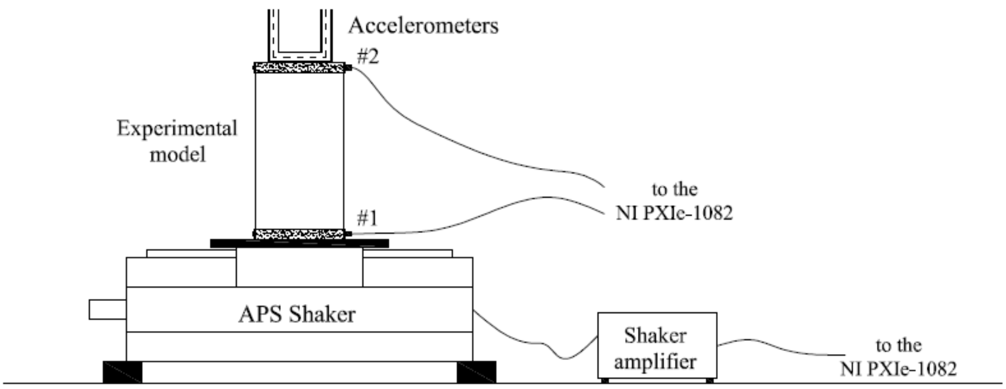

Fig. 4 Experimental setup

Table 1 Main systems dynamic parameters

	Configuration #1	Configuration #2
M	2.057 kg	2.039 kg
C	$0.1535\,N\,s/m$	$0.1272\,N\,s/m$
K	$318.33\,N/m$	$317.58\,N/m$
ζ_1	0.003	0.0025
ω_1	12.44 *rad/s*	12.48 *rad/s*

For each configuration, 15 samples of broadband noise, in the range 0.5-15 Hz (3.14-94.25 rad/s) with duration of 50 s and sampling frequency of 1 kHz, have been generated and used as ground acceleration. In this way the corresponding mean FRF, for the considered configuration, has been computed.

Once obtained the sought FRFs, dynamic parameters have been identified for each configuration using well-known techniques (Maia and Silva 1997, Ewins 1984) such as half-power bandwidth method and Rational Fractional Polynomial method. All these techniques leaded to similar results of the systems dynamic parameters, which are reported in Table 1.

In order to assess the reliability of the identified parameters, experimental vìs-a-vìs numerical mean FRFs are depicted in Fig. 5 for the two main systems configurations.

The perfect agreement between numerical and experimental results demonstrates the accuracy of the identified parameters in Table 1.

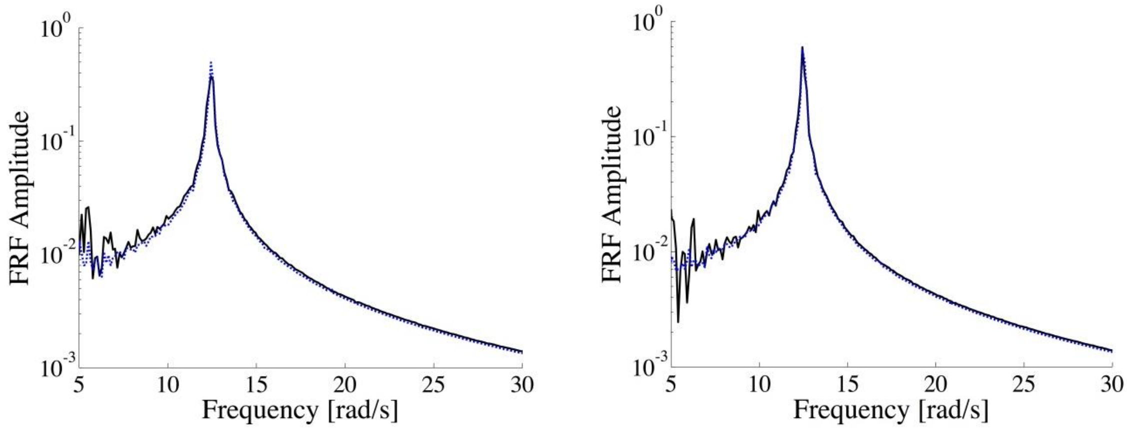

(a) FRF amplitude for Configuration #1 (b) FRF amplitude for Configuration #2

Fig. 5 Comparison of structural displacement mean FRFs for the main system: experimental results (black solid line), numerical results (blue dot line) using Eq. (3)

3.2 TLCD devices

Two configurations of TLCDs, with different cross sectional areas A, have been used. Further, vessels have been filled with water $\left(\rho = 1000\, kg/m^3\right)$ reaching different vertical liquid lengths h, to tune each TLCD with the corresponding main system configuration.

Figs. 6(a) and 6(b) show pictures of the two TLCD devices used for the tests, while in Figs. 6(c)-(d) schematic drawings of the TLCDs with the corresponding geometric dimensions are depicted.

The two TLCD configurations have been rigidly connected and excited at the base through an APS Dynamic-Model 133 shake table (Figs. 6(a) and 6(b)), while an accelerometer on the table itself has been used to acquire the ground acceleration.

For each device, 20 samples of broadband noise in the range 0.5-15 Hz (3.14-94.25 rad/s), with a duration of 25 s and sampling frequency of 1 kHz, have been generated and used as ground accelerations.

During the motion, a video camera (model Nikon D3200) has been employed to record the TLCD free surface vertical liquid displacements. Specifically, the camera was rigidly connected through a screw to the table to create a moving reference frame, integral with the TLCD devices. The camera has been positioned so that it focused on the left TLCD column, in order to record the liquid vertical displacements only (see Fig. 7 for a schematic view of the acquisition system).

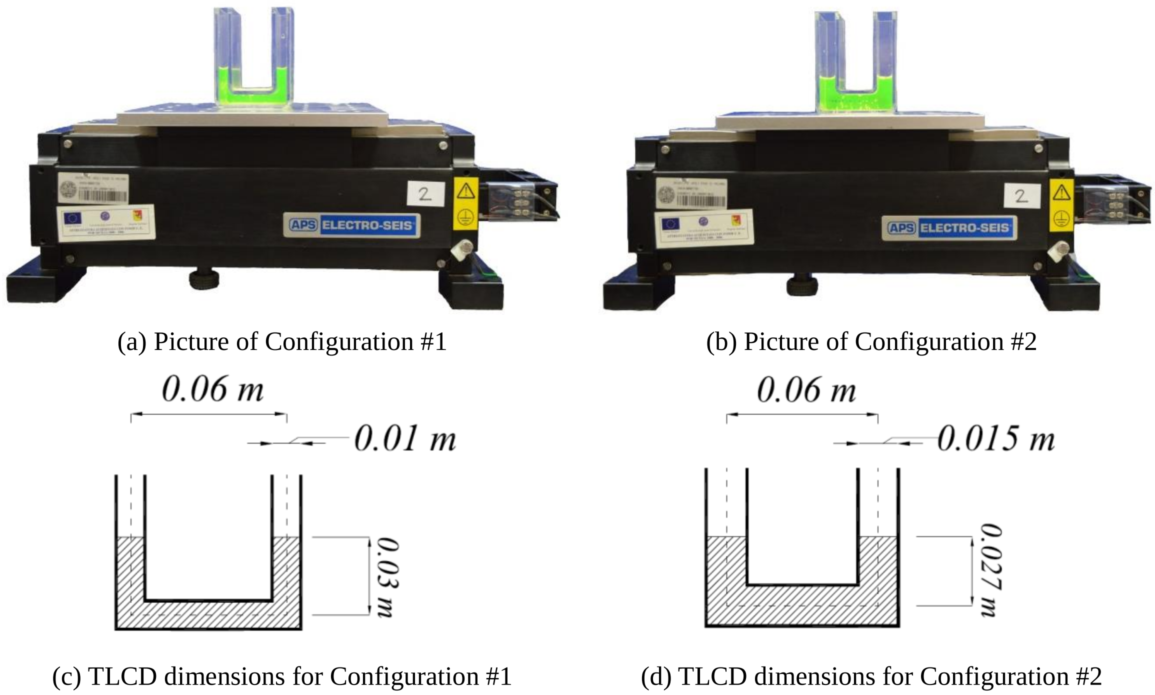

Fig. 6 TLCD devices

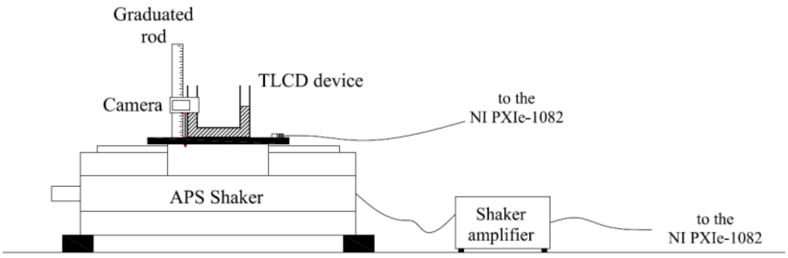

Fig. 7 Acquisition system for TLCDs tests

Each video, for every base acceleration sample, has been recorded at 30 fps (corresponding to a sampling frequency of 30 Hz) and high-resolution full-frame images of 1280×720 pixels have been acquired and transferred to the computer. Finally, in order to determine the free water surface displacements for each configuration, an image processing method in MATLAB environment has been used. Readers are referred to (Di Matteo *et al.* 2014b) for a description of the implemented image processing procedure.

Once base accelerations have been acquired and liquid vertical displacements time histories have been extracted from the videos, the mean FRFs of the two TLCDs configurations have been computed. The experimental natural frequency of oscillation of the liquid ω_{exp} has been directly identified from the corresponding FRF, while the head loss coefficient ξ has been determined by minimizing the gap between the experimentally measured liquid FRF and that obtained numerically solving Eq. (1), considering as input the recorded accelerations.

Table 2 TLCD geometric parameters

	Configuration #1	Configuration #2
d	0.01 m	0.015 m
A	$1 \cdot 10^{-3}\, m^2$	$1.5 \cdot 10^{-3}\, m^2$
b	0.06 m	0.06 m
w	0.014 m	0.021 m
γ	0.23	0.35
h	0.03 m	0.027 m
L	0.12 m	0.114 m
m	0.119 kg	0.182 kg
ω_e	12.78 rad/s	13.11 rad/s

Table 3 TLCD identified parameters

	Configuration #1	Configuration #2
ω_{exp}	18.35 *rad/s*	16.71 *rad/s*
ξ	12	10
β	0.0287	0.045
C_β	37.96	19.53

Further, in order to evaluate the TLCD parameters of the theoretical fractional model (β and C_β) in Eq. (6), a best fitting procedure, based on a nonlinear least square curve fitting method using MATLAB, has been applied to fit the experimental FRFs data with the one in Eq. (9).

The geometric and identified TLCD parameters, for each configuration, are detailed in Tables 2 and 3 respectively.

In order to assess the reliability of the identified parameters, numerical-experimental comparison of the liquid displacements mean FRF is depicted in Fig. 8, for each TLCD configuration. Note that, in this picture experimental FRFs are compared with those computed with Eq. (1) (say classical nonlinear formulation results) using the theoretical natural frequency ω_e in Eq. (2), and those computed numerically integrating Eq. (6) (say proposed fractional formulation results) using as parameters those reported in Tables 2 and 3. In both cases, the recorded accelerations have been used as input.

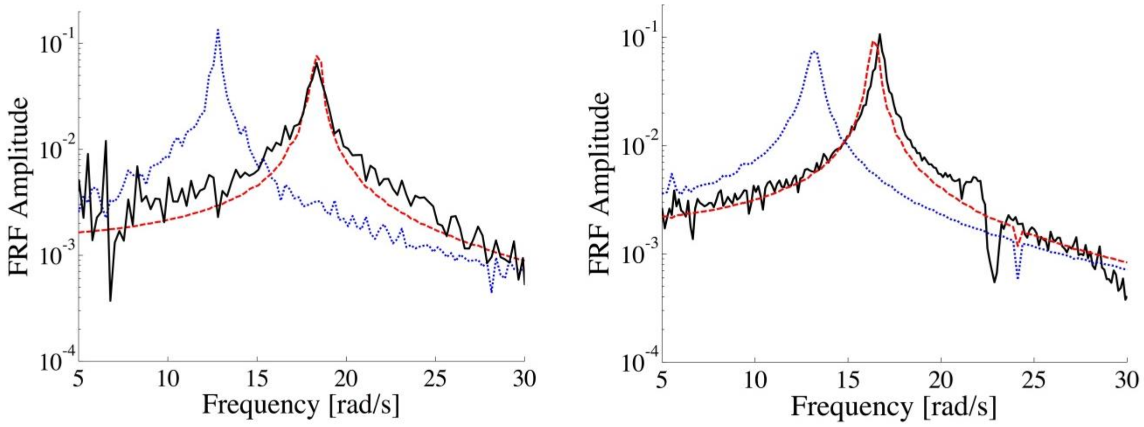

(a) FRF amplitude for Configuration #1 (b) FRF amplitude for Configuration #2

Fig. 8 Comparison of liquid displacement mean FRFs: experimental results (black solid line), classical nonlinear formulation results (blue dot line) and proposed fractional formulation results (red dashed line)

The satisfactory agreement between proposed fractional model and experimental curves shows that the dynamical parameters have been correctly identified. On the other hand, a rather evident discrepancy can be observed between the classical nonlinear model FRFs and the experimental ones. This is due to the differences between the theoretical natural frequency ω_e and the experimentally identified one ω_{exp}, as shown in Tables 2 and 3 as well. As in fact been demonstrated in other studies (Chaiviriyawong *et al.* 2007, Di Matteo *et al*. 2015b), this discrepancy may be due to the sloshing phenomenon which takes place when some particular geometrical configuration of the TLCD device are employed. On the other hand, as shown in (Di Matteo *et al.* 2014b), Eq. (1) leads to very good agreement among experimental and numerical results when the identified natural frequency ω_{exp} is used, together with the experimentally determined head loss coefficient ξ.

4. TLCD controlled systems: experimental validation of the proposed fractional formulation

Once main systems and TLCD devices parameters have been identified (see Tables 1-3), the validity of the proposed theoretical fractional model Eqs. (10) has been proved through several experimental tests on two TLCD controlled systems configurations, as outlined in the following.

In this regard pictures of the two systems configurations are shown in Figs. 9(a) and 9(b) while in Figs. 9(c) and 9(d) their schematic drawings are reported with the corresponding dimensions.

The two configurations have been excited at the base with the APS Dynamic-Model 133 shake table, through broadband noises in the range 0.5-15 Hz (3.14-94.25 rad/s) and duration of 50 s. Specifically 15 samples of broadband noise for each configuration have been generated, accelerations at the ground and at the upper plate have been recorded and the two mean FRFs have been computed.

As previously done for the TLCD devices only, once the two mean FRFs of the TLCD controlled structures have been obtained, a best fitting procedure has been applied to identify TLCD parameters for the theoretical fractional model (β and C_β). Therefore a nonlinear least square curve fitting method using MATLAB, has been applied to fit the two mean experimental FRFs with the corresponding theoretical ones given in Eq. (12). Quite remarkably, identified values of β and C_β matches those obtained using the TLCD devices only and reported in Table 3, thus further proving the correctness of the procedure outlined in Section 3.2.

To assess the validity of the proposed theoretical fractional model in Eqs. (10), numerical-experimental comparison of mean FRFs and relative structural accelerations are depicted in Figs. 10 and 11 for each TLCD controlled system configuration. Specifically in Figs. 10(a) and 10(b) the recorded relative upper plate accelerations are compared with those computed with Eq. (5) (say classical nonlinear formulation results) and those obtained numerically integrating Eq. (10) (say proposed fractional formulation results) using as parameters those reported in Tables 1-3.

Further in Figs. 11(a) and 11(b) the corresponding experimental and numerical mean FRFs are depicted. In all cases, the recorded accelerations have been used as input. It is worth noting that numerical classical results have been obtained with a 4th-order Runge-Kutta method, whereas numerical solution of Eq. (10) have been performed implementing a Newmark method through a discretization of the Caputo fractional derivative (Spanos and Evangelatos 2010, Failla and Pirrotta 2012), as detailed in Appendix A.

As shown for each configuration, proposed fractional model results closely match the corresponding experimental ones both in time and in frequency domain. In particular it is worth noting that in Fig. 11(b) proposed FRF (red dashed line) is almost fully coincident with the corresponding experimental one (black solid line).

(a) Picture of Configuration #1

(b) Picture of Configuration #2

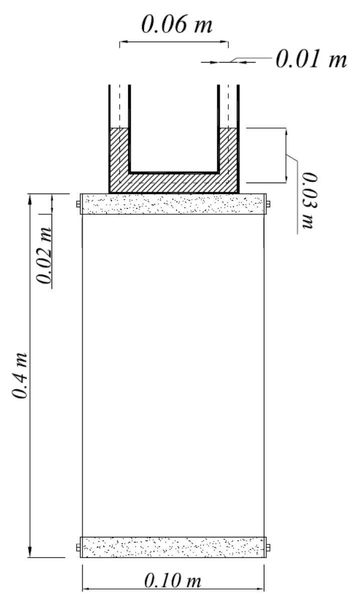

(c) Dimensions for Configuration #1

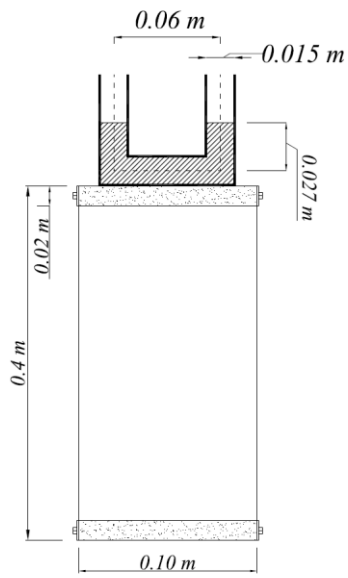

(d) Dimensions for Configuration #2

Fig. 9 Experimental setup of the controlled systems

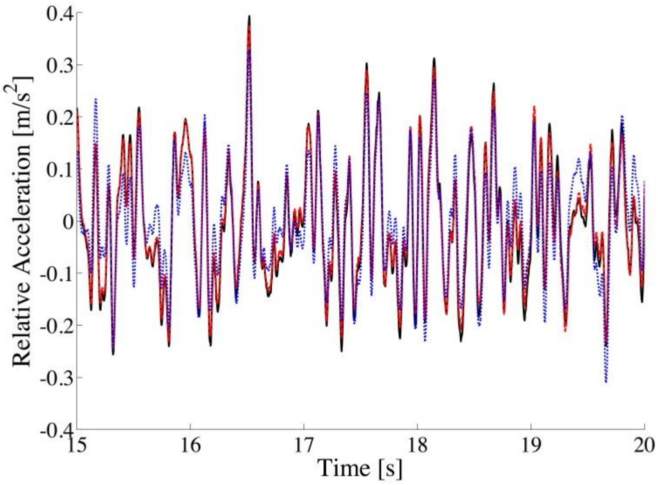

(a) Relative Acceleration for Configuration #1

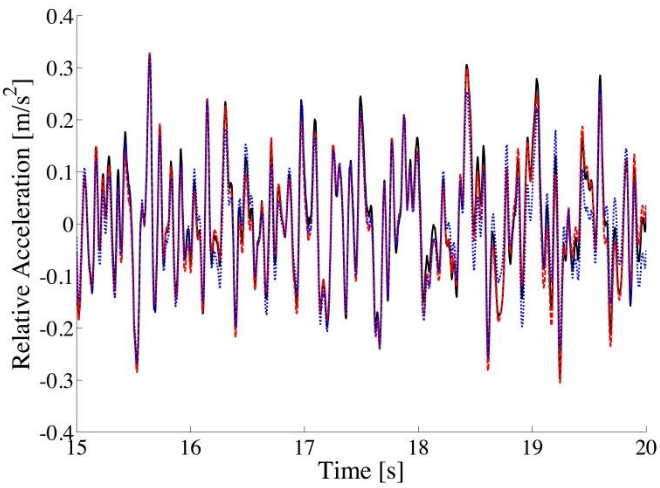

(b) Relative Acceleration for Configuration #2

Fig. 10 Comparison of relative upper plate accelerations: experimental results (black solid line), classical nonlinear formulation results (blue dot line) and proposed fractional formulation results (red dashed line)

On the other hand, as may be observed, numerical classical results are rather different from experimental data. This is due to the discrepancies between theoretical liquid natural frequency ω_e and the experimentally identified one ω_{exp}, which has been highlighted in previous section for the TLCD devices only. This discrepancy clearly reflects on the analysis of the TLCD controlled systems, leading to differences in detecting the second peak of the FRFs which is in fact associated to the TLCD devices. In this regard, higher differences can be observed in frequency domain, as shown in Fig. 11. This may represent a relevant result, since the great majority of studies on TLCD controlled structures deal with the optimal design parameter determination based on the classical nonlinear formulation, and generally working in the frequency domain.

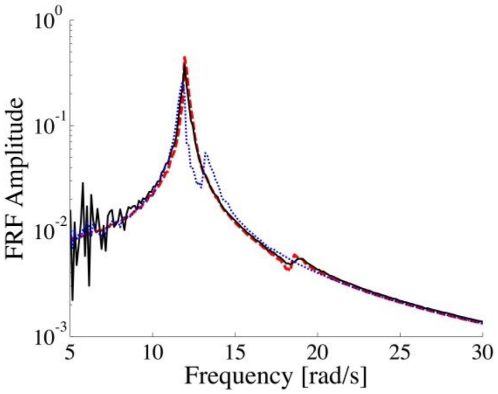

(a) FRF amplitude for Configuration #1

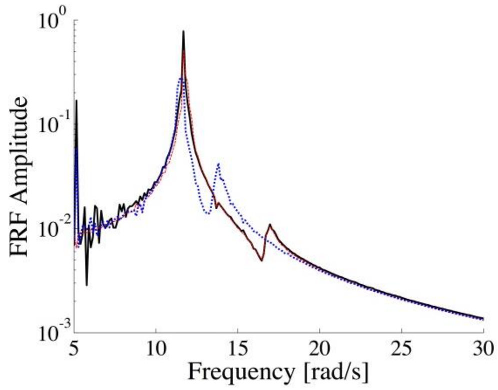

(b) FRF amplitude for Configuration #2

Fig. 11 Comparison of structural displacement mean FRFs: experimental results (black solid line), classical nonlinear formulation results (blue dot line) and proposed fractional formulation results (red dashed line)

4.1 Percentage discrepancy evaluation

In order to better evaluate the differences among experimental and numerical results, a properly percentage index has been introduced as

$$\varepsilon_i = \frac{\int_{t_i}^{t_f} \left[\ddot{x}_i^{th}(t) - \ddot{x}_i^{ex}(t) \right]^2 dt}{\int_{t_i}^{t_f} \ddot{x}_i^{ex}(t)^2 \, dt} \tag{15}$$

where $\left[t_i - t_f\right]$ is the observation window, $\ddot{x}_i(t)$ denotes the relative structural accelerations of the *i*-sample, while the apexes *th* and *ex* stand for numerical and experimentally measured, respectively. Clearly, as shown in Eq. (15), the greater the value of ε_i the higher the discrepancy.

Therefore, values of the index in Eq. (15) for the two analyzed TLCD controlled systems configurations have been computed for each sample considering both classical nonlinear formulation results (Eq. (5)) and proposed fractional formulation results (Eq. (10)). Figs. 12(a) and 12(b) show the trend of ε_i for the 15 samples of Configuration #1 and #2.

Further, to get an overview of these results, the mean discrepancies for each model has been computed as reported in Table 4, where e_c stands for the mean discrepancy of the classical model and e_f stands for mean discrepancy of the proposed fractional formulation.

As shown in Table 4, mean discrepancies obtained considering the proposed formulation are always smaller than those obtained from the classical one, thus proving that Eq. (10) can captures the real motion of TLCD controlled structures.

Table 4 Mean value of the discrepancies

	Configuration #1	Configuration #2
e_c	12.9%	12.8%
e_f	3.6%	6.5%

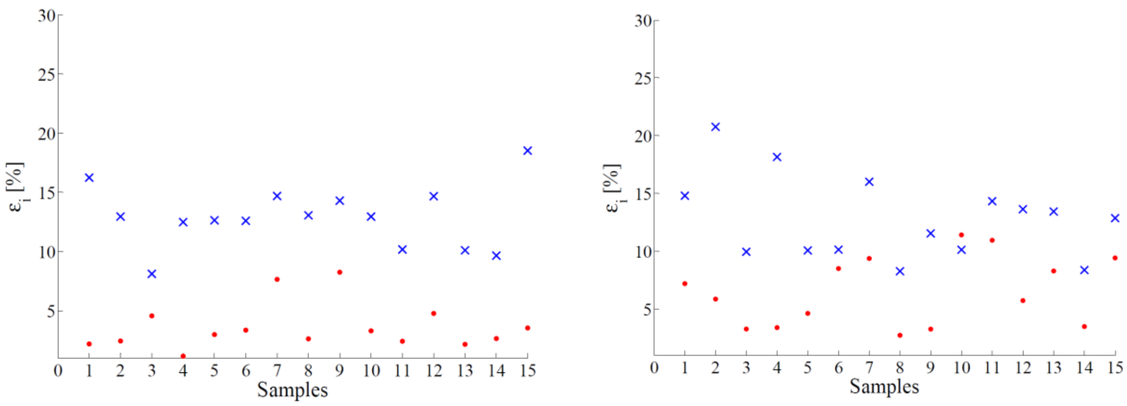

(a) ε_i for Configuration #1 (b) ε_i for Configuration #2

Fig. 12 Percentage values of ε_i for the 15 samples: numerical classical results (blue crosses) and proposed fractional model (red dots)

5. Conclusions

Recently, an alternative formulation, based on fractional operators, has been proposed to model liquid vertical displacements in TLCD devices, notably improving the prediction of the real liquid surface displacements with respect to the classical nonlinear model used in literature.

In this paper this alternative formulation has been extended to the case of TLCD controlled structures. Since the proposed fractional model is linear, identification of involved parameters is extremely simpler than the classical nonlinear one.

Further, the proposed fractional formulation has been validated by means of experimental tests on two different models realized in the Laboratory of Experimental Dynamic at University of Palermo. The two configurations were characterized by two different values of the ratio between the corner to corner width and the horizontal liquid length of the TLCD device, which has been proven to be an important parameter causing discrepancies among theoretical and experimental natural frequencies.

Numerical results obtained with the proposed fractional formulation have been compared with the corresponding experimental ones and numerical results computed with the classical nonlinear model.

Results show that responses obtained via the proposed fractional formulation highly match experimental data of the two tested TLCD controlled structures configurations, both in time and frequency domain. On the other hand, classical nonlinear formulation may lead to inadequate discrepancies among experimental and numerical responses, especially in frequency domain. This is a rather interesting result, since most researches in this field are focused on the determination of optimal design parameters based on the classical nonlinear formulation, working in frequency domain.

References

Chaiviriyawong, P., Webster, W.C., Pinkaew, T. and Lukkunaprasit, P. (2007), "Simulation of characteristics of tuned liquid column damper using a potential-flow method", *Eng. Struct.*, **29**, 132-144.

Cheng, C.W., Lee, H.H. and Luo, Y.T. (2015), "Experimental study of controllable MR-TLCD applied to the mitigation of structure vibration", *Smart. Struct. Syst.*, **15**, 1481-1501.

Di Matteo, A., Lo Iacono, F., Navarra, G. and Pirrotta, A. (2014a), "Direct evaluation of the equivalent linear damping for TLCD systems in random vibration for pre-design purposes", *Int. J. Nonlinear. Mech.*, **63**, 19-30.

Di Matteo, A., Lo Iacono, F., Navarra, G. and Pirrotta, A. (2014b), "Experimental validation of a direct pre-design formula for TLCD", *Eng. Struct.*, **75**, 528-538.

Di Matteo, A., Lo Iacono, F., Navarra, G. and Pirrotta, A. (2015a), "Optimal tuning of tuned liquid column damper systems in random vibration by means of an approximate formulation", *Meccanica*, **50**, 795-808.

Di Matteo, A., Lo Iacono, F., Navarra, G. and Pirrotta, A. (2015b), "Innovative modeling of tuned liquid column damper motion", *Commun. Nonlinear Sci. Numer. Simulat.*, **23**, 229-244.

Ewins, D.J. (1984), *Modal Testing: Theory And Practice*, Research Studies Press, Taunton, Somerset, England.

Failla, G. and Pirrotta, A. (2012), "On the stochastic response of fractionally-damped Duffing oscillator", *Commun. Nonlinear Sci. Numer. Simulat.*, **17**, 5131-5142.

Hitchcock, P.A., Kwok, K.C.S. and Watkins, R.D. (1997), "Characteristics of liquid column vibration absorbers (LCVA) – I", *Eng. Struct.*, **19**, 126-134.

Hochrainer, M.J. and Ziegler, F. (2006), "Control of tall building vibrations by sealed tuned liquid column dampers", *Struct. Control. Health Monit.*, **13**, 980-1002.

Ibrahim, R.A. (2005), *Liquid Sloshing Dynamics Theory And Applications*, Cambridge University Press, New York, NY, USA.

Konar, T. and Ghosh, A. (2013), "Bimodal vibration control of seismically excited structures by the liquid column vibration absorbers", *J. Vib. Control.*, **19**, 385-394

Lee, S.K., Lee, H.R. and Min, K.W. (2012), "Experimental verification on nonlinear dynamic characteristic of a tuned liquid column damper subjected to various excitation amplitudes", *Struct. Des. Tall Spec. Build.*, **21**, 374-388.

Lee, H.H. and Juang, H.H. (2012), "Experimental study on the vibration mitigation of offshore tension leg platform system with UWTLCD", *Smart. Struct. Syst.*, **9**, 71-104.

Maia, N.M.M. and Silva, J.M.M. (1997), *Theoretical And Experimental Modal Analysis*, Research Studies Press Ltd., John Wiley & Sons, New York, NY, USA.

Podlubny, I. (1999), *Fractional Differential Equations. An Introduction To Fractional Derivatives, Fractional Differential Equations, Some Methods Of Their Solution And Some Of Their Applications*, Academic Press, New York, NY, USA.

Sakai, F., Takeda, S. and Tamaki, T. (1989), "Tuned liquid column damper – new type device for suppression of building vibrations", *Proceedings of the International Conference on Highrise Buildings*.

Spanos, P.D. and Evangelatos, G.I. (2010), "Response of a non-linear system with restoring forces governed by fractional derivatives-time domain simulation and statistical linearization solution", *Soil Dyn. Earthq. Eng.*, **30**, 811-821.

Wu, J.C., Chang, C.H. and Lin, Y.Y. (2009), "Optimal design of non-uniform tuned liquid column dampers in horizontal motion", *J. Sound Vib.*, **326**, 104-122.

Wu, J.C., Shih, M.H., Lin, Y.Y. and Shen, Y.C. (2005), “Design guidelines for tuned liquid column dampers for structures responding to wind”, *Eng. Struct.*, **27**, 1893-905.

Wu, J.C., Wang, Y.P. and Chen, Y.H. (2012), “Design tables and charts for uniform and non-uniform tuned liquid column dampers in harmonic pitching motion”, *Smart. Struct. Syst.*, **9**, 165-188.

Yalla, S.K. and Kareem, A. (2000), “Optimum absorber parameters for tuned liquid column dampers”, *J. Struct. Eng. - ASCE*, **126**, 906-915.

Ziegler, F. (2007), “The tuned liquid column damper as a cost-effective alternative for the mechanical damper in civil engineering structures”, *J. Acoust. Vib.*, **12**, 25-39.

Ziegler, F. (2008), “Special design of tuned liquid column-gas dampers for the control of spatial structural vibrations”, *Acta Mech.*, **201**, 249-267.

Appendix A. Newmark method for the solution of the proposed fractional model

Since readers may not be familiar with the numerical solutions of fractional order differential equation, in this Appendix the numerical procedure used in this paper for the proposed fractional formulation Eq. (10) is outlined. Specifically, numerical results have been obtained implementing a Newmark method based on a Grunwald-Letnikov (GL) discretization (Podlubny 1999) of the Caputo fractional derivative in Eq. (7).

In this regard, considering a quiescent system at $(t=0)$ and subdividing the time interval $\left[0, t_f\right]$ into equally -spaced steps Δt, the fractional derivative Eq. (7) at time $(t_i = i\,\Delta t)$ can be approximated with the following GL series expansion

$$ {}_0^C D_t^\beta y(t) = \lim_{\Delta t \to 0} \Delta t^{-\beta} \sum_{k=0}^{i} GL_k \, y(t_i - k\Delta t) \tag{A.1} $$

where GL_k are coefficients to be computed recursively as

$$ GL_k = \frac{k-\beta-1}{k} GL_{k-1}, \quad GL_0 = 1 \tag{A.2} $$

Therefore, substituting Eq. (A.2) in Eq. (10), the equation of motion for the proposed fractional model at the time instant t_i can be rewritten as

$$ \begin{cases} (1+\mu)\ddot{x}(t_i) + \alpha\mu\ddot{y}(t_i) + 2\zeta_1\omega_1\dot{x}(t_i) + \omega_1^2 x(t_i) = -(1+\mu)\ddot{x}_g(t_i) \\ \alpha\ddot{x}(t_i) + \ddot{y}(t_i) + \dfrac{1}{2}\dfrac{C_\beta}{L}\Delta t^{-\beta} \displaystyle\sum_{k=0}^{i} GL_k \, y(t_i - k\Delta t) + \omega_e^2 y(t_i) = -\alpha\ddot{x}_g(t_i) \end{cases} \tag{A.3} $$

Specifying Eq. (A.3) for the following time instant t_{i+1} and subtracting from Eq. (A.3), yields

$$ \begin{cases} (1+\mu)\Delta\ddot{x} + \alpha\mu\,\Delta\ddot{y} + 2\zeta_1\omega_1\Delta\dot{x} + \omega_1^2\Delta x = -(1+\mu)\Delta\ddot{x}_g \\ \alpha\,\Delta\ddot{x} + \Delta\ddot{y} + \dfrac{1}{2}\dfrac{C_\beta}{L}\Delta t^{-\beta} GL_0 \Delta y + \omega_e^2 \Delta y = -\alpha\Delta\ddot{x}_g - \dfrac{1}{2}\dfrac{C_\beta}{L}\Delta t^{-\beta} P_i \end{cases} \tag{A.4} $$

where $(\Delta x = x(t_{i+1}) - x(t_i))$, $(\Delta y = y(t_{i+1}) - y(t_i))$, $(\Delta\ddot{x}_g = \ddot{x}_g(t_{i+1}) - \ddot{x}_g(t_i))$ and

$$ P_i = \sum_{k=1}^{i} GL_k \left[y(t_{i+1} - k\Delta t) - y(t_i - k\Delta t) \right] + GL_{i+1}\, y(0) \tag{A.5} $$

The term P_i can be then considered as a pseudo-force, depending on the liquid displacement until the time instant t_i.

Rewriting Eq. (A.4) in compact matrix form, yields

$$\tilde{\mathbf{M}}\Delta\ddot{\mathbf{Z}}+\tilde{\mathbf{C}}\Delta\dot{\mathbf{Z}}+\tilde{\mathbf{K}}\Delta\mathbf{Z}=-\tilde{\mathbf{A}}\Delta\ddot{x}_g-\tilde{\mathbf{B}} \tag{A.6}$$

where

$$\Delta\mathbf{Z}=\begin{bmatrix}\Delta x\\ \Delta y\end{bmatrix} \tag{A.6}$$

$$\tilde{\mathbf{M}}=\begin{bmatrix}1+\mu & \alpha\mu\\ \alpha & 1\end{bmatrix} \tag{A.7}$$

$$\tilde{\mathbf{C}}=\begin{bmatrix}2\zeta_1\omega_1 & 0\\ 0 & 0\end{bmatrix} \tag{A.8}$$

$$\tilde{\mathbf{K}}=\begin{bmatrix}\omega_1^2 & 0\\ 0 & a_\beta\end{bmatrix} \tag{A.9}$$

$$\tilde{\mathbf{A}}=\begin{bmatrix}1+\mu\\ \alpha\end{bmatrix} \tag{A.10}$$

$$\tilde{\mathbf{B}}=\begin{bmatrix}0\\ \frac{1}{2}\frac{C_\beta}{L}\Delta t^{-\beta}P_i\end{bmatrix} \tag{A.11}$$

$$a_\beta=\omega_e^2+\frac{1}{2}\frac{C_\beta}{L}\Delta t^{-\beta}GL_0 \tag{A.12}$$

In this way a classical Newmark scheme can be applied to find the numerical solution of the differential Eq. (A.6). Specifically, applying the constant average acceleration method the following relations hold true

$$\Delta\dot{\mathbf{Z}}=\frac{\Delta t}{2}\left[\ddot{\mathbf{Z}}(t_i)+\ddot{\mathbf{Z}}(t_{i+1})\right] \tag{A.13}$$

$$\Delta\mathbf{Z}=\Delta t\,\dot{\mathbf{Z}}(t_i)+\frac{\Delta t^2}{4}\left[\ddot{\mathbf{Z}}(t_i)+\ddot{\mathbf{Z}}(t_{i+1})\right] \tag{A.14}$$

in which $\mathbf{Z}(t_i)$ is the state variables vector

$$\mathbf{Z}(t_i)=\begin{bmatrix}x(t_i)\\ y(t_i)\end{bmatrix} \tag{A.15}$$

Substituting Eq. (A.13) and (A.14) into Eq. (A.6) and manipulating, yields

$$\ddot{\mathbf{Z}}\left(t_{i+1}\right)=\boldsymbol{\theta}^{-1}\left\{\left[\tilde{\mathbf{M}}-\frac{\Delta t}{2}\tilde{\mathbf{C}}-\frac{\Delta t^{2}}{4}\tilde{\mathbf{K}}\right]\ddot{\mathbf{Z}}\left(t_{i}\right)-\Delta t\,\tilde{\mathbf{K}}\,\dot{\mathbf{Z}}-\mathbf{A}\,\Delta\ddot{x}_{g}-\tilde{\mathbf{B}}\right\} \tag{A.16}$$

where

$$\boldsymbol{\theta}=\tilde{\mathbf{M}}+\frac{\Delta t}{2}\tilde{\mathbf{C}}+\frac{\Delta t^{2}}{4}\tilde{\mathbf{K}} \tag{A.17}$$

Clearly, once obtained the response acceleration vector $\ddot{\mathbf{Z}}\left(t_{i+1}\right)$ from Eq. (A.16), velocity and displacements responses can be determined through Eqs. (A.13) and (A.14).